Directional solidification cells at low velocities

Maurice Mashaal, Martine Ben Amar, and Vincent Hakim
Laboratoire de Physique Statistique, Ecole Normale Supérieure, 24 rue Lhomond, 75231 Paris CEDEX 05, France
(Received 10 October 1989)

Profiles of deep solidification cells are computed numerically in the framework of the one-sided model of directional solidification. Previous results obtained for a constant miscibility gap ($K=1$) are confirmed and extended to arbitrary K values for small Péclet numbers ($P \ll 1$). Various approximate relations between experimentally measurable quantities are deduced from a viscous finger analogy and tested numerically. We point out an effective parameter that should prove useful in comparing the miscellaneous experimental results.

INTRODUCTION

In directional solidification experiments, a dilute binary mixture is drawn at constant velocity U across a linear temperature gradient. Above a critical pulling speed U_c, the interface between the liquid and solid parts becomes cellular, with deep liquid grooves separating periodically spaced fingers of solid.[1] Aside from its intrinsic metallurgical importance, this phenomenon is a prototype pattern-forming system, where a complex nonlinear structure is created out of a simple shape (here the planar front) by an underlying instability: the Mullins and Sekerka instability[2] of crystal growth. It has thus attracted much interest (for a review, see Ref. 3). In particular, the question of wavelength selection has been considered numerically both for finite-amplitude cells[4,5] and deep cells.[6] We and others[5-7] have concluded that no preferred wavelength can be determined from a steady-state analysis, but that a well-defined shape is always obtained once the wavelength is fixed. Our previous results were restricted to the case of a constant miscibility gap[6,7] (partition coefficient equal to 1), and to the one-sided model of solidification where impurity diffusion is entirely neglected in the solid phase. The last restriction greatly simplifies the global analysis but does not seem to modify the cell shape.[5] In the present paper, the analysis is detailed and generalized to a gap varying linearly with the concentration of impurity. As previously, we focus on the regime where the impurity diffusion length l_d (given by $2D/U$, with D the diffusion coefficient in the liquid) is much greater than the cell wavelength α, both because it is an experimentally meaningful regime and because an analogy with the viscous fingering problem[8] can be pursued.[7,9]

Using this analogy, we have established approximate relations pointing out a unique and relevant dimensionless combination σ_{eff} of physical parameters and have checked them numerically. We have tried to present the different results, which *a priori* depend on several parameters, in a unified way. Some of the approximate derived relations have been already obtained by Billia and coworkers[1,10] on more phenomenological grounds by an extended compilation of experimental data in the cellular and dendritic regimes. We have summarized our main results and given the expressions of the relevant dimensionless quantities in the first part of this paper for the convenience of the reader that is not interested in the details of our analytical and numerical techniques. Sections II and III contain our derivations of these results. In Sec. II, we show how the analogy with viscous fingering can help to extract the relevant parameters. Section III is devoted to a detailed exposition of our numerical method, based upon the Green's-function technique, a useful tool to solve the free-boundary problem.

I. NUMERICAL RESULTS AND APPROXIMATE RELATIONS

It is usual to gather the different parameters which describe a directional solidification experiment into the following four typical lengths.

(i) The spatial periodicity α.

(ii) The impurity diffusion length in the liquid phase $l_d=2D/U$.

(iii) The thermal length l_t as given by $m\Delta C_0/G$ with m the absolute value of the slope of the liquidus, G the temperature gradient, and ΔC_0 the miscibility gap at the melting temperature of the planar interface. We consider a phase diagram where the miscibility gap is either constant or linearly dependent on the melting temperature. The former case corresponds to a segregation coefficient K (Ref. 11) equal to 1, the latter to a coefficient smaller than 1.

(iv) The capillary length d_0 arising from the Gibbs-Thomson relation with $d_0=T_f^0\gamma/Lm\Delta C_0$, γ being the surface tension, T_f^0 the melting temperature of the pure material, and L the latent heat.

This choice is the minimal one and it supposes that several simplifying hypotheses have been made. We have neglected solutal diffusion in the solid phase and thermal diffusion due to the released latent heat in both phases. We have assumed equality of heat capacity for the liquid and the solid phase. Finally we have hidden the anisotropy of surface tension ϵ in d_0. The physical meaning of these lengths come from the Mullins and Sekerka stabili-

ty analysis[2] of the planar solidification front which demonstrates the destabilizing role of the impurities diffusion and the stabilizing effect of both the thermal gradient and the surface tension. With these four lengths, we can construct three independent parameters, such as the Péclet number P, the dimensionless ratio ν, and the capillary constant σ:

$$P=2\alpha/l_d,\quad \nu=\frac{l_t}{l_d},\quad \sigma=d_0 l_t/\alpha^2 . \tag{1.1}$$

Above the instability threshold ($\nu=\frac{1}{2}$ with our conventions if one neglects surface tension corrections), the interface becomes cellular and we want to describe the shape of the individual cells and the effective parameters on which they depend.

The analogy between cells of directional solidification and Saffman-Taylor (ST) fingers is now well known.[7,9] For small Péclet numbers and on a length scale of the order of the cell spacing, the cell tip is well represented by a Saffman-Taylor finger, while for distances greater than $1/P$, the asymptotic tail behavior is reached. In order to describe the cell profile, one should understand which viscous finger shape is to be chosen for given parameters (P,ν,σ) of a solidification experiment. When such a correspondence can be made, the cell shape is described by a single effective parameter corresponding to the single parameter σ_{ST} determining the viscous finger profile. Before explaining this, let us first recall some known results concerning viscous fingering.

A. Selection of finger shape

When one injects air in a linear Hele-Shaw cell filled with oil, the planar interface between air and oil is unstable and after a transient period the interface takes the form of a long finger of air moving at a constant speed along the middle axis of the cell.[8,3] The finger profile can be entirely characterized by the ratio λ of the finger width to the cell width. The relative width λ depends on the experimental conditions but only as a function $F(\sigma_{ST})$ of the dimensionless surface tension coefficient σ_{ST}. σ_{ST} is given by the ratio $b^2T/(48\mu Ua^2)$ where b is the Hele-Shaw plates spacing, a their half-width, μ the viscosity of the driven fluid, U the constant velocity of the interface, and T the surface tension. Approximate formulas can be obtained for the finger shape and the function F in the two limits of small or large σ_{ST}.

When σ_{ST} is small, the shape is only weakly modified by capillary effects and is conveniently represented by the analytical profile discovered by Saffman and Taylor:[8]

$$y(x)=\frac{\lambda}{\pi}\arccos\exp[-\pi x/(1-\lambda)] . \tag{1.2}$$

Here and in the following, the distances are measured in units of the cell spacing α. As shown by several authors,[12,13] λ is related to σ_{ST}, for small σ_{ST} values, by

$$\lambda-\tfrac{1}{2}=F(\sigma_{ST})-\tfrac{1}{2}\approx 2.98\sigma_{ST}^{2/3} . \tag{1.3}$$

If the surface tension anisotropy ϵ is neglected, λ is always greater than $\frac{1}{2}$, and λ tends to $\frac{1}{2}$ when σ_{ST} tends to zero. Ordinary values of ϵ (≤ 0.1) modify the selection function F only at very small surface tension[14] (our precise definition of anisotropy is to be found after Eq. 3.6).

The analytical results [(1.2) and (1.3)] are no more valid as soon as σ_{ST} grows. In the strong surface tension limit[7,15] (equivalent to $\lambda\to 1$), the viscous finger can be described in two parts: the tip and the tail. The tip is given in term of a pendulum function

$$x(\theta)\approx\sqrt{2\sigma_{ST}}(1-\sqrt{\cos\theta}) , \tag{1.4a}$$

$$y(\theta)\approx\sqrt{\sigma_{ST}/2}\int_0^\theta d\tau\sqrt{\cos\tau}\quad\text{with } 0\leq\theta\leq\pi/2 . \tag{1.4b}$$

As expected in this limit, capillary effects strongly affect the shape of the tip and the predicted shape [Eq. (1.4)] is very different from the Saffman-Taylor analytical profile [Eq. (1.2)] in the $\lambda\to 1$ limit. The former is rather convex while the latter is completely flat. Since the y coordinate of the finger is bounded by $\frac{1}{2}$ (the half-width of the Hele-Shaw cell), Eq. (1.4b) implies that σ_{ST} cannot be greater than $\sigma_{max}\approx 0.35$ and at strong surface tension the relative width λ reads[7]

$$\lambda=F(\sigma_{ST})\approx 1-\left[\frac{(\sigma_{max}-\sigma_{ST})}{2.17}\right]^{3/2} . \tag{1.5}$$

Between these two limits which can be handled analytically, i.e., for arbitrary σ_{ST} values, a numerical investigation has to be performed. We have solved the free-boundary problem by use of the Green's-function techniques as described in Sec. III and we have computed the F function plotted in Fig. 2 in complete agreement with the results of Ref. 13.

B. Correspondence between a viscous finger and a solidification cell

The above results on viscous fingering being recalled, we can proceed and give the correspondence between a cell defined by the three independent parameters ν, P, and σ and a Saffman-Taylor finger defined either by λ or σ_{ST}. As explained above the relative width λ of a Saffman-Taylor finger is a known function of σ_{ST}, $\lambda=F(\sigma_{ST})$. Our result is that, when the viscous finger analogy holds, we have the corresponding relation in directional solidification

$$\lambda=F(\sigma_{eff}) , \tag{1.6a}$$

where λ is the relative width of the Saffman-Taylor finger fitting the tip of the solidification cell and σ_{eff} is an effective combination of the different experimental parameters whose expression is given by[16]

$$\sigma_{eff}=\frac{1-(1-K)\lambda}{K}\frac{\sigma}{2\nu-1} . \tag{1.6b}$$

It is important to stress that the function F which appears in (1.6a) is the same as the function F which appears in the Saffman-Taylor problem. Note that this expression has been obtained first[17] from a marginal stability criterion. Before proceeding to testing numerically Eqs. (1.6), we should explain how to measure λ since this

quantity does not have an obvious meaning for directional solidification cells. The hidden λ parameter can be measured either from the asymptotic behavior of the profile in the groove or from the geometry of the cell tip. Let us begin by examining the first possibility. The profile in the groove depends on the partition coefficient K. If K is less than 1, it obeys Scheil's law:[11]

$$y(x)\sim\tfrac{1}{2}-Ax^{-\beta} \text{ with } \beta=1/(1-K)\ , \tag{1.7a}$$

while the $K=1$ case gives

$$y(x)\sim\tfrac{1}{2}-A\exp(-\mu x) \text{ with } \mu=P/(2\nu-1)\ . \tag{1.7b}$$

Our choice of coordinates is illustrated in Fig. 1. The value of A has been determined in the $K=1$ case[7] by matching the two representations—the Saffman-Taylor finger tip and the asymptotic groove—in their common domain of validity:

$$A=(1-\lambda)/2 \tag{1.7c}$$

with λ the relative width of the Saffman-Taylor finger. Therefore a determination of the profile in the groove provides a way of measuring the hidden parameter λ in the $K=1$ case.[6] The same strategy can be followed for $K<1$. A matching between the tip and the tail region determines the arbitrary constant A in (1.7a) and gives (see Sec. II)

$$y(x)\sim\frac{1}{2}-\frac{(1-\lambda)}{2}\left[\frac{1+(1-K)\mu x}{1+(1-K)\mu x_{\text{tip}}}\right]^{-\beta} \tag{1.7d}$$

with $\beta=1/(1-K)$ and $\mu=P/(2\nu-1)$. Therefore, as in the $K=1$ case, one can extract A numerically from the asymptotics in the cusp and deduce the λ parameter associated with a given cell. It is then possible to compute λ for the profiles obtained numerically (as explained in Sec. III) for given values of (P,ν,σ) and test the validity of relations (1.6). This is shown in Fig. 2 and the comparison between Figs. 2(a) and 2(b) gives a numerical evidence in favor of this relation, since the gap between curves of different K values is significantly reduced. A slight disagreement remains, probably due to our numerical way of obtaining a precise value of λ when P is not equal to zero. The possible different cell shapes are shown in Fig. 3 as function of σ_{eff}. At fixed K, Fig. 4 proves that the selection function F is rather weakly dependent on P, for small P values. The small discrepancy linear in P is not surprising, since relations (1.6) are established in the vanishing Péclet number limit and are valid up to corrections linear in P. The influence of the Péclet number is also shown in Fig. 5, where it can be seen that the separation between the tail and tip regions tends to disappear as P increases. Finally, in Fig. 6, we have plotted some profiles with the same σ_{eff} for different K values. The tips are identical and the shapes differ only in the tails in agreement with Eq. (1.7). This leads us to the second way

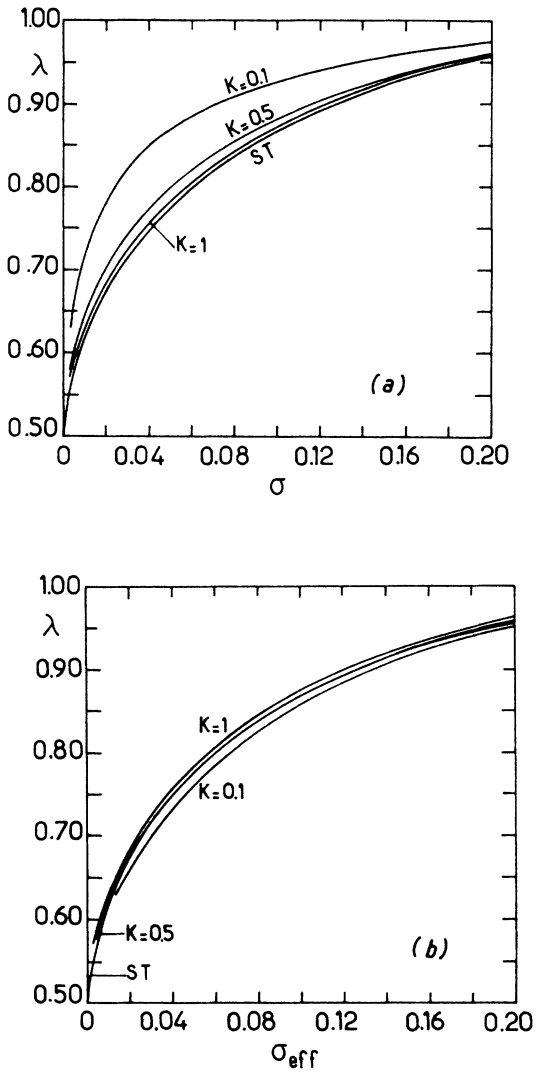

FIG. 2. (a) λ as a function of σ for viscous fingering (ST) and for directional solidification ($P=0.1$, $\nu=1$) at different values of K. (b) λ as a function of σ_{eff} for the same cases.

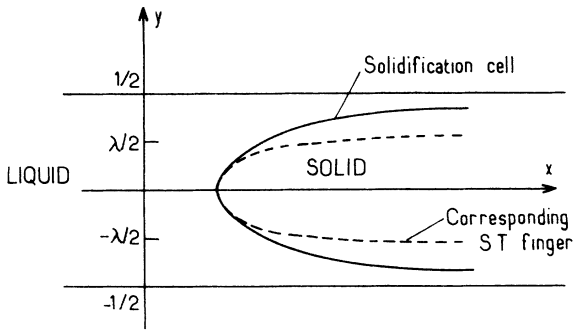

FIG. 1. Sketch of a cell showing the coordinates system used.

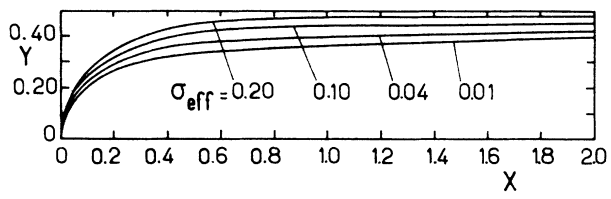

FIG. 3. Half-cell profiles for $K=0.1$, $P=0.1$, and $\nu=1$ at different values of σ_{eff}.

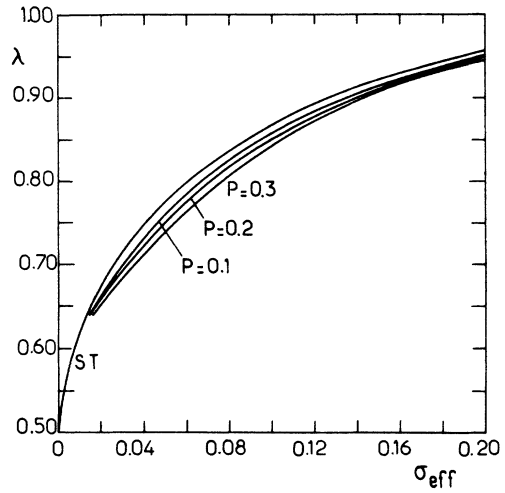

FIG. 4. λ as a function of σ_{eff} for $P=0$ (Saffman-Taylor fingering) and $P=0.1, 0.2, 0.3$ ($K=0.1$, $\nu=1$).

of determining λ. The idea is that when a Saffman-Taylor finger and a cell tip are superimposable they have the same tip radius of curvature. So if one wants to associate a λ parameter to a given cell one can measure its tip radius of curvature and take the relative width λ of the related viscous finger. In order to apply this alternative strategy one needs the relation between λ and the tip radius of curvature for Saffman-Taylor fingers. Analytical predictions are known at low and strong surface tensions.

(i) When $\sigma \to 0$, one can calculate the tip curvature from Eq. (1.2)

$$\frac{\alpha}{R_0} = \frac{\pi(1-\lambda)}{\lambda^2} \quad \text{with} \quad \lambda \approx 0.5 \; . \tag{1.8a}$$

(ii) When $\sigma \to \sigma_{\max}$, one obtains[7]

$$\frac{\alpha}{R_0} = \left[\frac{2}{\sigma_{\max}} \left[1 + \frac{3.2}{(4\sigma_{\max})^{1/3}} (1-\lambda)^{2/3} \right] \right]^{1/2}$$

$$\text{if } \lambda \approx 1, \quad \sigma_{\max} \approx 0.35 \; . \tag{1.8b}$$

Between these two limits, the relation between the tip curvature and λ (or σ_{eff}) for Saffman-Taylor fingers must be computed and is represented in Fig. 7. Also in this figure are presented the tip curvature of our cells for different values of the partition coefficient K at fixed P.

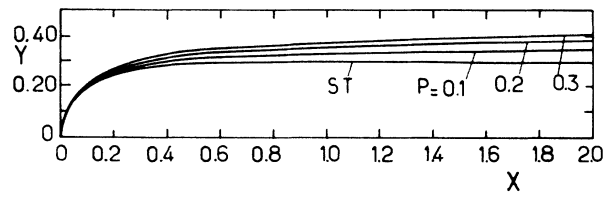

FIG. 5. Half-cell profiles for $\sigma_{\text{eff}}=0.007$ at different Péclet numbers. $P=0$ is the Saffman-Taylor case; the three other curves are at $K=0.5$ and $\nu=1$.

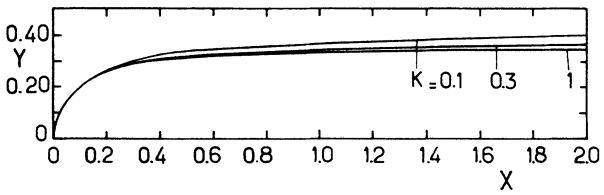

FIG. 6. Half-cell profiles for $\sigma_{\text{eff}}=0.01$, $P=0.1$, and $\nu=1$ at different values of K.

All the curves nicely overlap. This strategy for obtaining λ is probably the best one if one wants to test experimentally relations (1.6). Unfortunately, since the value of the tip radius is always confined between two limits [2.39,6.28] in the cellular regime according to (1.7), the deduced λ values may be difficult to obtain with high precision. A partial experimental test of relations (1.6) can already be found in the work of Billia and co-workers.[10] They have not really plotted σ_{eff} but instead $\sigma/(2\nu-1)$ (with their notations $1/F^{1/2}$) versus the dimensionless tip radius, for different concentrations of the succinonitrile-acetone alloy (with $K=0.1$). The plot (which includes the results of different experiments done by various authors[18]) covers different values of our typical lengths d_0, l_t, l_d but for the same alloy and therefore for the same value of K. All the experimental results can be fitted to a unique curve, as expected if σ_{eff} is the good parameter which selects the tip radius. The global shape of the curve in the cellular regime also seems compatible with our prediction. Nevertheless, additional data in the cellular regime is needed if one wants to test the K dependence of relations (1.6). It has been noted[19] in some regime of parameters that a modification of wavelength changes

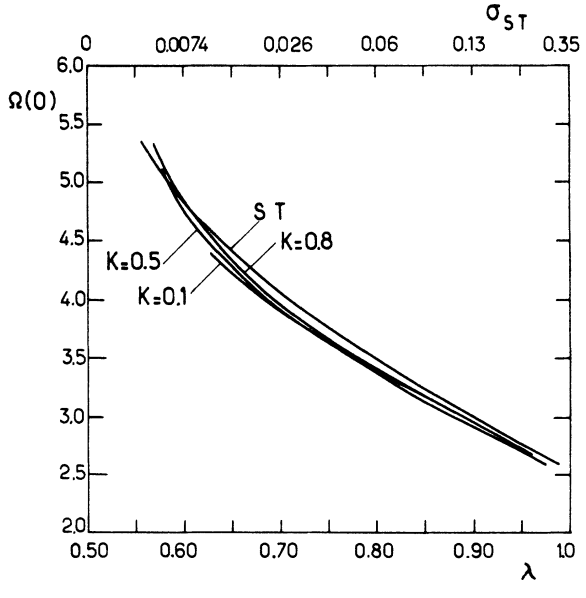

FIG. 7. The curvature at the tip as a function of λ for Saffman-Taylor fingers and for directional solidification ($P=0.1$, $\nu=1$) at different values of K.

cell profiles only by a global rescaling. This seems to occur far from the planar threshold but within the cellular regime. This similarity of profiles at different drawing velocities could also result from relations (1.6). The wavelength α is not an adjustable parameter and it varies empirically with the pulling speed U as $\alpha \approx U^{-1/2}$. The cell similarities can be explained as follows. Two experiments achieved at different velocities are characterized by the same $\sigma/2\nu$ (equal to $d_0 D/U\alpha^2$). As a consequence, they have the same σ_{eff} (if one can neglect 1 compared to 2ν) and thus the same dimensionless tip radius R_0/α. So R_0 scales as the wavelength α. This explanation and its conclusion are no more valid near the planar threshold and at the cell-dendrite transition.[1]

The comparison between computed and experimental cell shape that we have envisaged until now requires a rather sophisticated experiment with camera equipment. Most of the experiments achieved in the past are not so sophisticated but give a lot of available data. The useful compilation of Ref. 10 points out two important measured quantities, the aforementioned dimensionless tip radius (the cell spacing is used as length unit) and the tip shift x_{tip} relative to the planar front position in the temperature gradient G. These two quantities are strongly dependent on the global shape of the cell and before concluding this section, we would like to summarize our results for the second quantity.

C. The tip shift

When U increases above its threshold value, the tip moves in the temperature gradient in order to ensure the impurities conservation relation. Let us note this displacement x_{tip}. If one chooses the x axis along the pulling speed U and oriented toward the cold part of the cell, one has the mean relation [see Eq. (2.7) below]

$$\langle x \rangle + \sigma \langle \Omega \rangle = 0 , \tag{1.9}$$

where Ω is the curvature of the interface and the average $\langle\ \rangle$ is taken over one period of the pattern. This equation gives a way to calculate x_{tip} if the shape of the interface is known. From an experimental point of view, x_{tip} can be measured either directly or estimated by the measure of the tip temperature, especially in alloys. Our result for x_{tip} is well represented by the formula

$$\frac{x_{\text{tip}}}{\alpha} = -\frac{2\nu-1}{P}\frac{1-\lambda}{1+(K-1)\lambda} + \frac{2\nu-1}{\nu}\sigma . \tag{1.10}$$

So, the cell tip raises in the thermal gradient as the velocity is increased from its threshold value. This result depends on the Saffman-Taylor parameter λ. The first term on the right-hand side of (1.10) is mainly due to the cusp tail, and thus does not depend on the details of the tip shape. This term is the dominant one in the small Péclet limit and its expression is derived in Sec. II. This is not the case for the correction of order σ [the second term on the right-hand side of (1.10)], which is subdominant in this limit and out of reach for our analysis valid to leading order in P. In fact, from the analysis of Sec. II, we would expect this correction to depend on the shape of the cell. Our numerical results are nonetheless consistent with a correction equal to $(2\nu-1)\sigma/\nu$ as shown in Fig. 8. The correction term has been fitted with highest accuracy in the range of small $(1-\lambda)$ since it is negligible as soon as P is small compared to $(1-\lambda)$ (σ being restricted to the interval $[0,(2\nu-1)\sigma_{\max}]$). μx_{tip} has no Péclet dependence as shown in Fig. 8, so its measure gives precise λ values in the cellular regime as mentioned in Refs. 1 and 10. If the surface tension is known, the selection function F can then be directly measured. Having summarized our results, let us present the analytical approaches which have been used for their derivation.

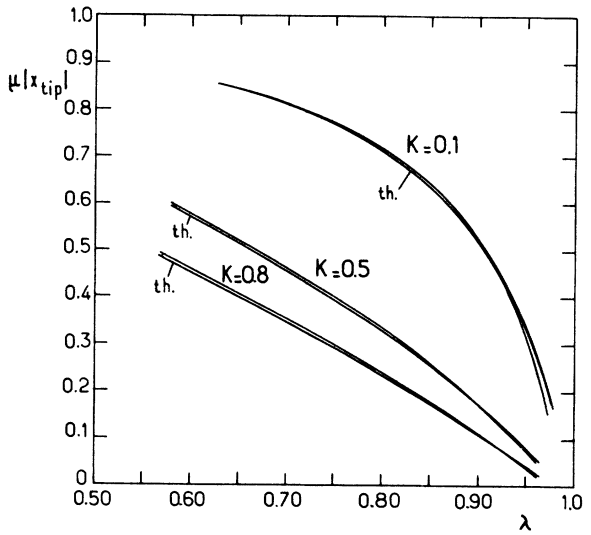

FIG. 8. $\mu|x_{\text{tip}}|$ as a function of λ for $K=0.1$, 0.5, and 0.8 ($P=0.1$, $\nu=1$). The curves indicated by "th." (theoretical value) are those given by (1.10). The case $K=0.1$ also shows the curves corresponding to $P=0.2$ and $P=0.3$.

II. ANALYTICAL APPROACH IN THE SMALL PÉCLET NUMBER LIMIT

In this section, we want to generalize to any K values (less than 1) the results of Refs. 5, 6 and 9 which are restricted to the case of a constant miscibility gap ($K=1$). We want to show that in the small Péclet number limit ($P \ll 1$), the tip region of the cell takes the form of a viscous finger whose effective surface tension parameter σ_{eff} is given by Eq. (1.6) above. We will use the same theoretical approach as in Refs. 7 and 15 so our analysis is valid in the strong surface tension limit. In fact, our numerical results prove the approximate validity of our findings in the whole surface tension range. An alternative theoretical approach[20] has been proposed in the limit of vanishing K values but for an arbitrary Péclet number. Our results show that the cell shapes do not depend separately on the various experimental and material parameters, but only on the combination σ_{eff}, which is therefore the important one for the comparison of different experimental results. This has also been emphasized in Ref. 10 on more phenomenological grounds.

Let us first recall the basic equations of directional solidification[3] in the framework of the one-sided model, where the chemical diffusion in the solid is neglected.

In the bulk, the relative impurity excess $u(x,y)=[C(x,y)-C_\infty]/\Delta C$ obeys the stationary diffusion equation:

$$\frac{\Delta U}{\Delta U}-P\frac{\partial u}{\partial x}=0 , \tag{2.1a}$$

while on the interface, one must apply both the Stefan and the Gibbs-Thomson laws:

$$[K+(1-K)u_{\rm int}]P\cos\theta=-(\mathbf{n}\cdot\nabla u)_{\rm int} , \tag{2.1b}$$

$$u_{\rm int}=1+\frac{P}{2\nu}(x_{\rm int}+\sigma\Omega) , \tag{2.1c}$$

where $u_{\rm int}$ means the u quantity evaluated at the interface, θ the angle between the normal at the interface and the growth direction, and $\Omega=y''/(1+y'^2)^{3/2}$ the curvature of the interface. Due to our choice of coordinates, some signs in (2.1) may be different in comparison from more standard formulations.

In order to show the analogy with viscous fingering, it is convenient to introduce a new diffusion field ϕ related to u by

$$\phi=\frac{2\nu}{P}(u-1)-x . \tag{2.2}$$

The previous set (2.1) becomes

$$\Delta\phi-P\frac{\partial\phi}{\partial x}=P , \tag{2.3a}$$

$$[(2\nu-1)+(1-K)P(\phi+x)_{\rm int}]\cos\theta=-(\mathbf{n}\cdot\nabla\phi)_{\rm int} , \tag{2.3b}$$

$$\phi_{\rm int}=\sigma\Omega . \tag{2.3c}$$

On length scales of order 1 around the cell tip, the terms linear in P are negligible compared to the Laplacian in the diffusion equation (2.3a). Therefore, Eqs. (2.3) are identical to the Saffman-Taylor equations with $[\mu=P/(2\nu-1)]$

$$\sigma_{\rm eff}=\frac{\sigma}{(2\nu-1)[1+(1-K)\mu x_{\rm tip}]} \tag{2.4}$$

playing the role of the parameter $\sigma_{\rm ST}$ in viscous fingering. Note that according to (2.2) $x_{\rm tip}$ is expected to be of order $1/P$.

To proceed further, we estimate the position $x_{\rm tip}$ of the cell tip at dominant order in P; this is most easily done by using the impurity conservation law. Let us establish it by integrating Eq. (2.1a) in the melt domain Σ in front of the cell. This gives

$$0=\int\int_\Sigma dx\,dy\left[\Delta u-P\frac{\partial u}{\partial x}\right]$$
$$=\int\int_\Sigma dx\,dy\,\Delta u-P\int_{-1/2}^{1/2}dy\,u[x_{\rm int}(y)] , \tag{2.5}$$

where we have used the fact that u goes to zero as $x\to-\infty$. The integral of the Laplacian can be evaluated using the Gauss theorem:

$$\int\int_\Sigma dx\,dy\,\Delta u=\int_{\partial\Sigma}ds\,\mathbf{n}\cdot\nabla u$$
$$=P\int_{-1/2}^{1/2}dy[K+(1-K)u_{\rm int}] . \tag{2.6}$$

Impurity conservation can therefore be written as

$$0=K\int_{-1/2}^{1/2}dy(1-u_{\rm int})=-\frac{KP}{\nu}\int_0^{1/2}dy(x_{\rm int}+\sigma\Omega) . \tag{2.7}$$

We have taken into account the symmetry of the cells and recovered Eq. (1.9). At dominant order in P, the integral is evaluated by breaking it into two parts, a first one I_1 corresponding to the tip region (x from zero to $\lambda/2$), and a second one I_2 corresponding to the groove (x from $\lambda/2$ to $+\infty$). In the first integral, x can be approximated by $x_{\rm tip}$ with the result

$$I_1=\frac{\lambda}{2}x_{\rm tip}+O(1) .$$

In the groove, the matching with the Saffman-Taylor corresponding finger proves that the asymptotic Sheil's law can be written as (see Appendix A)

$$y(x)\sim\frac{1}{2}-\frac{(1-\lambda)}{2}\left[\frac{1+(1-K)\mu x}{1+(1-K)\mu x_{\rm tip}}\right]^{-\beta}$$
$$\text{with } \beta=\frac{1}{1-K} . \tag{2.8}$$

The matching procedure can be justified rigorously only when $(1-\lambda)$ is small. The estimate (2.8) can be used to evaluate I_2 and this gives

$$I_2=\frac{(1-\lambda)}{2\mu(1-K)}\{[1+(1-K)\mu x_{\rm tip}]/K-1\}+O(1) .$$

Therefore, we finally obtain the tip position as given before in Eq. (1.10):

$$\mu x_{\rm tip}=-\frac{1-\lambda}{1-(1-K)\lambda}+O(P) .$$

If we use this estimation of the tip position, we obtain the desired expression (1.6) for $\sigma_{\rm eff}$

$$\sigma_{\rm eff}=\frac{1-(1-K)\lambda}{K}\frac{\sigma}{2\nu-1} .$$

We have therefore justified at small Péclet numbers and strong surface tension ($\sigma_{\rm eff}\to\sigma_{\rm max}$) the approximate relations used in Sec. I. Our numerical results explained in Sec. I show that the last limitation is not a real one, since all the approximate relations are numerically satisfied for arbitrary σ values.

III. GREEN'S-FUNCTION FORMULATION AND NUMERICAL SCHEME

This part is devoted to the numerical determination of the cell profile. In order to solve the diffusion equation with its nonlinear boundary conditions on the unknown interface, we use the Green's-function technique. As for the needle-crystal growth,[21] this gives a convenient way to handle the free-boundary problem. Contrary to Refs.

5 and 22, we do not restrict ourselves to the $K=1$ case. So, let us recall the integral equation to solve, within the one-sided model framework, for an arbitrary partition coefficient K. The symmetric Green's function can be found in Ref. 22. Hereafter, we use an approximate expression valid when $(P/4\pi)^2 \ll 1$, which makes the computation faster:

$$G(q_0,q)=\frac{1}{P}(e^{-(P/2)(x-x_0+|x-x_0|)}-1) - \frac{1}{4\pi}e^{(P/2)(x_0-x)}\ln\lambda_- + \text{c.c.} \quad (3.1a)$$

where

$$\lambda_\pm = 1-\exp 2\pi[i(y_0 \pm y)-|x_0-x|] . \quad (3.1b)$$

The Green's function obeys the usual differential equation

$$\Delta G(q_0,q)+P\frac{\partial G}{\partial x}(q_0,q)=-\delta(x_0-x)\delta(y_0-y) . \quad (3.2)$$

Here q and q_0 mean arbitrary points of the liquid phase $q=(x,y)$ and $q_0=(x_0,y_0)$. In order to find an equation valid for the interface, one integrates the quantity $[u(q)\Delta G(q_0,q)-G(q_0,q)\Delta u(q)]$ over the liquid phase domain Σ, fixing the point q_0 on the interface defined by $y(x)$. Using Green's second theorem (10.714 of Ref. 23) and the diffusion equation, one derives

$$\frac{u(q_0)-1}{2}=-\int_0^\infty dx\frac{ds}{dx}\tilde{G}(q_0,q)\hat{\mathbf{n}}\cdot\nabla_q u-\int_0^\infty dx\,[u(q)-1][y'P\tilde{G}(q_0,q)-\hat{\mathbf{n}}\cdot\nabla_q\tilde{G}(q_0,q)(1+y'^2)^{1/2}] . \quad (3.3)$$

In (3.3) q_0 and q represent interface points and y' represents the first derivative of the interface profile with respect to x. Here, we have chosen the origin of coordinates at the cell tip and taken into account the cell symmetry about the x axis (the half-cell profile has been supposed monotonic in order to integrate over the x variable). We have put

$$\tilde{G}(q_0,q)=\frac{2}{P}[e^{(P/2)(x-x_0+|x-x_0|)}-1] - \frac{1}{4\pi}e^{(P/2)(x_0-x)}(\ln\lambda_+ +\ln\lambda_-)+\text{c.c.} \quad (3.4)$$

Taking into account the Gibbs-Thomson (2.16) and the Stefan (2.1c) laws one finally obtains

$$\frac{w(q_0)}{2}=2v\int_0^\infty dx\,y'\tilde{G}(q_0,q)-\int_0^\infty dx\,w(q)[y'P\tilde{G}(q_0,q)-\hat{\mathbf{n}}\cdot\nabla_q\tilde{G}(q_0,q)(1+y'^2)^{1/2}]+(1-K)\int_0^\infty dx\,w(q)y'P\tilde{G}(q_0,q) , \quad (3.5)$$

with $w(q)=(2v/P)(u-1)=x+x_{\text{tip}}+\sigma\Omega$. Here, x_{tip} explicitly appears since we have chosen the origin of coordinates at the cell tip. It represents the shift of the tip position relative to the planar front interface in the temperature gradient. x_{tip} is implicitly given by the impurity conservation relation (2.7):

$$\int_0^\infty dx\,y'w=\int_0^\infty dx\,y'(x+x_{\text{tip}}+\sigma\Omega)=0 , \quad (3.6)$$

and depends thus on the profile function solution to Eq. (3.3). In Ω, we can include anisotropy of surface tension. Here, we choose a four-fold anisotropy which is not unrealistic for polymer materials used in solidification experiments,[1] so hereafter Ω means

$$\Omega \rightarrow \Omega(1-\epsilon\cos 4\theta) ,$$

where θ is the angle between the normal at the interface and the x axis, and (3.6) gives

$$x_{\text{tip}}=2\left[\sigma(1+\epsilon/15)+\int_0^\infty dx\,[y(x)-\tfrac{1}{2}]\right] . \quad (3.7)$$

The major difficulty in numerically solving integro-differential equations like (3.3) comes from the integrand singularities when $q=q_0$. In Eq. (3.3) the most severe one is given by the gradient term $(x+x_{\text{tip}})\nabla_q G$, in the asymptotic part of the cell ($x\rightarrow\infty$). It is only in this region, as shown in Sec. II and Appendix A, that we can extract the λ value, important to characterize the cell shape. This is why a careful treatment is necessary when $x\rightarrow\infty$, as developed below. In particular, to suppress the gradient term mentioned above, we have established an exact identity valid for any function describing a symmetric cell:

$$(x_0+x_{\text{tip}})/2=\int_0^\infty dx\,y'\tilde{G} - \int_0^\infty dx\,(x+x_{\text{tip}})[y'P\tilde{G} -(1+y'^2)^{1/2}\hat{\mathbf{n}}\cdot\nabla\tilde{G}] + P\int\int_\Sigma dx\,dy\,G . \quad (3.8)$$

This is obtained by integrating

$$\nabla\cdot[(x+x_{\text{tip}})\nabla G]$$

over the domain Σ, using Gauss's divergence theorem. Note that if we set $P=0$ (viscous fingering), we recover the identity [Eq. (4) of Ref. 22] established by Karma for the same purpose. Subtracting (3.5) from (3.8) we get

$$-\tfrac{1}{2}\sigma\Omega(x_0)=(1-2v)\int_0^\infty dx\,y'\tilde{G} + \sigma\int_0^\infty dx[y'P\tilde{G}-\hat{\mathbf{n}}\cdot\nabla\tilde{G}(1+y'^2)^{1/2}]\Omega(x) + P\int\int_\Sigma dx\,dy\,G + (K-1)\int_0^\infty dx\,y'P\tilde{G}(x+x_{\text{tip}}+\sigma\Omega) . \quad (3.9)$$

The last equation can be written in terms of "elementary" integrals already introduced in Ref. 6 for the $K=1$ case. Let us recall their definitions for convenience:

$$Z_{\pm}=\int_0^{\infty} dx\, y' e^{(P/2)(x_0-x)}\ln\lambda_{\pm} ,$$
$$Z_{\pm}^{*}=\sigma\int_0^{\infty} dx\, y'\Omega e^{(P/2)(x_0-x)}\ln\lambda_{\pm} ,$$
$$Y_{\pm}=i\int_0^{\infty} dx\, \epsilon(x_0-x) e^{(P/2)(x_0-x)}\ln\lambda_{\pm} , \tag{3.10}$$
$$Y_{\pm}^{*}=i\sigma\int_0^{\infty} dx\, \epsilon(x_0-x)\left[\frac{d\Omega}{dx}-\frac{P}{2}\Omega\right] e^{(P/2)(x_0-x)}\ln\lambda_{\pm} ,$$
$$X_{\pm}=\int_0^{\infty} dx\, xy' e^{(P/2)(x_0-x)}\ln\lambda_{\pm} .$$

[$\epsilon(x)$ is the sign of x.] With these notations, the integral equation (3.9) becomes

$$\sigma\Omega(x_0)[1-2y(x_0)]+2(I_1-2\nu I_2-\sigma J_1)+\frac{1}{2\pi}\mathrm{Re}\left[(2\nu+1)(Z_{+}+Z_{-})-\frac{P}{2}(Z_{+}^{*}+Z_{-}^{*})-2(Y_{+}-Y_{-})-(Y_{+}^{*}-Y_{-}^{*})\right]+(K-1)\left[2[I_1-I_2+PI_3+\sigma(J_2-J_1)]-\frac{P}{2\pi}\mathrm{Re}(X_{+}+X_{-}+Z_{+}^{*}+Z_{-}^{*})+Px_{\mathrm{tip}}\left[2I_2-\frac{1}{2\pi}\mathrm{Re}(Z_{+}+Z_{-})\right]\right]=0 , \tag{3.11}$$

with

$$I_1=\int_{x_0}^{\infty} dx\,[y-y(\infty)] ,$$
$$I_2=\int_{x_0}^{\infty} dx\,[y-y(\infty)]e^{P(x_0-x)} ,$$
$$I_3=\int_{x_0}^{\infty} dx\, x[y-y(\infty)]e^{P(x_0-x)} , \tag{3.12}$$
$$J_2=\int_{x_0}^{\infty} dx\, y'\Omega e^{P(x_0-x)} ,$$
$$J_1=\int_{x_0}^{\infty} dx\, y'\Omega = -(1+\epsilon/15)+\frac{1}{(1+y_0'^2)^{1/2}}\times\left[1-\epsilon+\tfrac{8}{3}\epsilon\frac{1}{1+y_0'^2}-\tfrac{8}{5}\epsilon\frac{1}{(1+y_0'^2)^2}\right] .$$

Some new integrals had to be defined because the partition coefficient is different from 1. To recover the integral equation for the Saffman-Taylor case, one has to specify the following values:

$$P=0,\quad \nu=1,\quad K=1,\quad y(\infty)=\lambda/2 .$$

The numerical procedure for solving the integral equation consists in writing a discretized version at every point x_0 of an adequate mesh. The resulting nonlinear system for the unknowns $y_i=y(x_i)$ is then solved by Newton's method. This method requires a zeroth-order profile to initialize the numerical procedure, before iterations. Although rather powerful, it needs good estimates for some limiting values of the parameter ($\nu\approx 0.5$ or $\sigma\approx 0.35$). So we take advantage of the analytical results made explicit in Sec. II. We recall that, for small P numbers, the neighborhood of the tip can be fitted by a Saffman-Taylor finger. Moreover, the trial function must behave correctly in the grooves. In Appendix B, we prove that the solution of the integral equation (3.11) exhibits the same asymptotic behavior as the one predicted by Eq. (1.7). Nevertheless, we must consider two cases according to the value of the partition coefficient.

(i) If $K=1$, we choose a parametrized zeroth-order profile given by

$$y_{\lambda}^{(0)}(x)=\frac{1}{\pi}[1+(\lambda-1)e^{-\mu x}]\arccos\left[\exp\left[-\frac{\pi x}{1-\lambda}\right]\right] \tag{3.13}$$

for small or vanishing surface tension. One can check that $y_{\lambda}^{(0)}(x)$ looks like the Saffman-Taylor finger for $x<1$, and verifies (1.7b) at large x. When σ is equal to zero, the numerical solutions are very close to (3.13) when P is not too large ($P<1.5$), for any value of the λ parameter between zero and 1. With a different choice of the trial function $y_{\lambda}^{(0)}(x)$, after some iterates, our code converges to a solution close to (3.13). From the computed solution λ is extracted at large distances from the tip by use of relation (1.7c). Note that we never obtain λ parameters less than zero, although λ is not physically restricted to the interval [0,1] in directional solidification (contrary to the Saffman-Taylor case), if one ignores the theoretical analysis explained above. For large surface tension, as for the viscous fingering case, a more appropriate tip profile in terms of the pendulum function has been chosen in agreement with (1.4). This choice improves the trial function and makes the iteration procedure quicker and more efficient.

(ii) If $K<1$, the trial function for small surface tension is built in the same way as for the $K=1$ case, taking into account (1.7d):

$$y_{\lambda}^{(0)}(x)=\frac{1}{\pi}[1+(\lambda-1)(1+\alpha_0 x)^{-\beta}]\times\arccos\left[\exp\left[-\frac{\pi x}{1-\lambda}\right]\right] ,$$

with

$$\beta=\frac{1}{1-K},\quad \alpha_0=\frac{\mu}{\beta+\mu x_{\mathrm{tip}}^{(0)}} ,$$

$x_{\rm tip}^{(0)}$ being computed either by Eq. (3.7) applied to $y_\lambda^{(0)}(x)$, or given by (1.9). Both ways give almost the same value. As for the previous case, this function set has to be modified for large surface tension.

To implement Newton's method, the infinite x interval $[0,+\infty[$ is first mapped into the finite u interval [0,1], on which a uniform mesh is defined. The mapping $x(u)$ is chosen such that $x\sim u^2$ when $u\to 0$, so at the origin y behaves like $x^{1/2}$ and represents a suitable physical cell profile. The integrals containing $\ln\lambda_\pm$ present logarithmic singularities at $x\sim x_0$ (or $u\sim u_0$) which have to be subtracted before numerical computation. For example, we write

$$Z_\pm=\int_0^1 du\,[\tilde{y}' e^{(P/2)(x_0-x)}\ln\lambda_\pm-\tilde{y}'_0\ln\tilde{\lambda}_\pm^*]+\tilde{y}'_0\int_0^1 du\,\ln\tilde{\lambda}_\pm^*\ ,$$

$$Y_\pm=i\int_0^1 du\,\epsilon(u_0-u)[x'(u)e^{(P/2)(x_0-x)}\ln\lambda_\pm-x'_0\ln\tilde{\lambda}_\pm^*]+ix'_0\int_0^1 du\,\epsilon(u_0-u)\ln\tilde{\lambda}_\pm^*$$

with

$$\tilde{y}'=\frac{dy}{du}\ .$$

In $\lambda_\pm$, we have developed to first order the exponent around u_0:

$$\tilde{\lambda}_+^*=1-\exp 2\pi[2iy_0-i(u_0-u)\tilde{y}'_0-|u_0-u|x'_0]\ ,$$

$$\tilde{\lambda}_-^*=1-\exp 2\pi[i(u_0-u)\tilde{y}'_0-|u_0-u|x'_0]\ .$$

This allows us to calculate analytically the substracted integrals in terms of the dilog function[25] as shown in Ref. 6. Similar treatments have been applied to the other integrals and are necessary to extract the λ parameter from the tail. Since we cannot define precisely where the asymptotic laws begin to be valid outside of the $P=0$ limit, our λ parameters are defined up to corrections linear in P. This may explain the linear dispersion in P apparent in Fig. 4.

CONCLUSION

We have presented the results of a numerical computation of the steady-state cells seen in directional solidification, in the low-velocity regime. We have shown that the numerical results can be described using a single effective parameter. This has been explained by an analogy with viscous fingering. This use of an effective parameter should help to compare different experimental results in a meaningful way and may provide a basis for relations which have been discovered empirically.[10] Two main unsettled issues in directional solidification are the understanding of wavelength selection and the cell-to-dendrite transition. An extension of the present work to Péclet numbers of order 1 is needed to address the second one and see if the transition corresponds to a critical value of the effective parameter. This remains a task for future studies.

ACKNOWLEDGMENTS

We are grateful to Bachir Moussallam for many valuable discussions and advice on the computational work. We would also like to thank Bernard Billia for sending copies of his work prior to publication. This research was supported by the Centre National d'Etudes Spatiales, by a grant, Incitation à la Recherche 1988, Grant No. N01236 and by the Direction des Recherches Etudes et Techniques, Grant No. 88 C 0219.

APPENDIX A: MATCHING EQUATION BETWEEN THE TIP AND THE GROOVE REGIONS

An equation is needed for interpolating between the Saffman-Taylor-like tip region and the Scheil asymptotic deep in the groove. This has been done in Ref. 7 for a partition coefficient K equal to 1 along the lines of Landau and Levich's classical analysis[24] of the coating film problem. The easy generalization to the $K\neq 1$ case is given here for the convenience of the reader. It has also been found in Ref. 20 independently of us.

Let us denote the small quantity $\frac{1}{2}-y(x)$ by $h(x)$. In the region considered, the curvature is approximately given by $-d^2h/dx^2$. Equation (2.3c) reads, therefore,

$$\phi(x,h(x))=-\sigma\frac{d^2h}{dx^2}\ ,$$

or by differentiation

$$\frac{\partial\phi}{\partial x}+\frac{dh}{dx}\frac{\partial\phi}{\partial y}=-\sigma\frac{d^3h}{dx^3}\ . \tag{A1a}$$

On the other hand, (2.3b) can be written approximately as

$$\frac{\partial\phi}{\partial x}\frac{dh}{dx}-\frac{\partial\phi}{\partial y}=\frac{dh}{dx}\left[(2\nu-1)-P(1-K)\left[\sigma\frac{d^2h}{dx^2}-x\right]\right]\ . \tag{A1b}$$

The derivative of the field ϕ on the interface can then be expressed in terms of the interface profile by solving Eqs. (A1). This gives, with the same approximation,

$$\frac{\partial\phi}{\partial x}=-\sigma\frac{d^3h}{dx^3}\ , \tag{A2a}$$

$$\frac{\partial\phi}{\partial y}=-\frac{dh}{dx}\left[(2\nu-1)-P(1-K)\left[\sigma\frac{d^2h}{dx^2}-x\right]\right]-\sigma\frac{dh}{dx}\frac{d^3h}{dx^3}\ . \tag{A2b}$$

These boundary conditions can now be used to solve perturbatively the diffusion equation (2.3a), taking into account the slow variation of ϕ along the x axis (the axis of the groove).

Let us write

$$\phi=\phi_0+\phi_1+\cdots\ .$$

At zeroth order, the diffusion equation reduces to

$$\frac{\partial^2\phi_0}{\partial y^2}=0\quad\text{or}\quad\phi_0=yA(x)+B(x)\ .$$

The reflection symmetry about the middle of the groove and the boundary condition (A2a) on the interface give $A(x)=0$, $B(x)=-\sigma d^2h/dx^2$.

The first-order correction to ϕ can now be computed. The diffusion equation reads at this order

$$\frac{\partial^2\phi_1}{\partial y^2}=P-\frac{\partial^2\phi_0}{\partial x^2}+P\frac{\partial\phi_0}{\partial x}$$

or

$$\frac{\partial\phi_1}{\partial y}=y\left[P-\frac{\partial^2\phi_0}{\partial x^2}+P\frac{\partial\phi_0}{\partial x}\right].$$

The compatibility of this last equation with the boundary condition (A2b) on the interface gives the equation for the profile of the groove that can be matched with the tip region:

$$\sigma\frac{d}{dx}\left[h\frac{d^3h}{dx^3}\right]=\frac{dh}{dx}[1-2v-P(1-K)x]-Ph+\sigma P\left[h\frac{d^3h}{dx^3}+(1-K)\frac{dh}{dx}\frac{d^2h}{dx^2}\right].$$

In the asymptotic region, the linear terms are dominant and one recovers Scheil's asymptotic result Eq. (1.1). In the tip region ($Px\ll 1$) one recovers the inner equation of the Saffman-Taylor problem. Matching between those two domains determines the constant of Scheil's power law to be $(1-\lambda)/2$ in the tip region [Eq. (2.8)] as discussed in Ref. 7.

APPENDIX B: ASYMPTOTICS FROM THE INTEGRAL EQUATION

In this appendix, we show how to obtain the asymptotic behavior of the cell profile $y(x)$ directly from the integro-differential equation (3.11). Again we must distinguish two cases, according to the K value. The $K=1$ is somewhat tedious since almost all the integrals of Eq. (3.11) contribute to the asymptotic behavior. At the same time, we examine the Saffman-Taylor case and recover McLean and Saffman's results.[13] The $K<1$ case is straightforward.

1. $K=1$

In this case we, look for an asymptotic behavior of the form

$$y(x)\sim y(\infty)-Ae^{-\mu x} \tag{B1}$$

as $x\to\infty$, where A and μ are constants, and $y(\infty)=\frac{1}{2}$ ($\lambda/2$ in the Saffman-Taylor case). Taking this form, the asymptotic behaviors of the integrals I_n and J_n appearing in (3.12) are elementary to find. For example,

$$I_1(x_0)=\int_{x_0}^{\infty}dx\,[y-y(\infty)]\sim-\frac{A}{\mu}e^{-\mu x_0}.$$

The integrals containing $\ln\lambda_\pm$ are somewhat more involved, and we choose Z_- as an example. To obtain its asymptotic behavior, we expand the logarithm and split the integration domain at x_0 to write

$$Z_-(x_0)=-\sum_{n=1}^{\infty}\frac{1}{n}\left[\int_{x_0}^{\infty}dx\,y'e^{(P/2+2\pi n)(x_0-x)}e^{2\pi ni(y_0-y)}+\int_0^{x_0}dx\,y'e^{(P/2-2\pi n)(x_0-x)}e^{2\pi ni(y_0-y)}\right].$$

In the first integral on $[x_0,\infty[$, we can take $y_0-y\approx 0$, so we get easily

$$\int_{x_0}^{\infty}dx\,y'e^{(P/2+2\pi n)(x_0-x)}e^{2\pi ni(y_0-y)}\sim\frac{\mu A}{2\pi n+(\mu+P/2)}e^{-\mu x_0}.$$

The second integral on $[0,x_0]$ can be written

$$\int_0^{x_0}dx\,y'e^{(P/2-2\pi n)(x_0x)}e^{2\pi ni(y_0-y)}=e^{(P/2-2\pi n)x_0}e^{2\pi niy_0}f(x_0)$$

where

$$f(x_0)=\int_0^{x_0}dx\,y'e^{-(P/2-2\pi n)x}e^{-2\pi niy}.$$

To obtain the behavior of $f(x_0)$, we differentiate it with respect to x_0:

$$f'(x_0)=y'(x_0)e^{-(P/2-2\pi n)x_0}e^{-2\pi niy(x_0)}.$$

For x large, $y(x)$ is nearly constant, so that by integrating back we find, using $y'\sim\mu A\exp(-\mu x)$,

$$f(x_0)\sim\frac{\mu A}{2\pi n-(\mu+P/2)}e^{-(\mu+P/2-2\pi n)x_0}\times e^{-2\pi niy_0}+\text{const},$$

and therefore

$$\int_0^{x_0}dx\,y'e^{(P/2-2\pi n)(x_0-x)}e^{2\pi ni(y_0-y)}\sim\frac{\mu A}{2\pi n-(\mu+P/2)}e^{-\mu x_0}.$$

Thus, we have, with $\mu_P=\mu+P/2$,

$$Z_-(x_0)\sim-4\pi\mu Ae^{-\mu x_0}\sum_{n=1}^{\infty}\frac{1}{4\pi^2n^2-\mu_P^2}.$$

This series has a closed-form expression (see Sec. 1.445 of Ref. 23), and we finally get

$$\mathrm{Re}Z_-(x_0)\sim Z_-(x_0)\sim-\pi A\mu/\mu_P[2/\mu_P-\cot(\mu_P/2)]e^{-\mu x_0}. \tag{B2}$$

The same treatment can be applied to Z_+, leading to the series

$$\sum_{n=1}^{\infty} \frac{e^{i4\pi n y(\infty)}}{4\pi^2 n^2 - \mu_P^2} ,$$

whose real part has also a closed-form expression (Sec. 1.445 of Ref. 23), giving thus

$$\mathrm{Re}Z_+(x_0) \sim -\pi A \frac{\mu}{\mu_P} \left[\frac{2}{\mu_P} - \frac{\cos\{[1-4y(\infty)]\mu_P/2\}}{\sin(\mu_P/2)} \right] e^{-\mu x_0} . \quad \text{(B3)}$$

The dominant behavior of $Y_\pm$ can be obtained in an analogous manner, except that $\exp 2\pi n i(y_0 \pm y)$ needs to be expanded one order beyond the constant term. For directional solidification $[y(\infty)=\frac{1}{2}]$, we get

$$\mathrm{Re}Y_\pm(x_0) \sim -2\pi A e^{-\mu x_0} \sum_{n=1}^{\infty} \left[\frac{P}{4\pi^2 n^2 - (P/2)^2} \pm \frac{2\mu_P}{4\pi^2 n^2 - \mu_P^2} \right] , \quad \text{(B4)}$$

where the series can be computed. One sees easily that the terms $\mathrm{Re}Y_\pm^*$ and $\mathrm{Re}Z_\pm^*$ are subdominant, and putting (B2)–(B4) into the integral equation (3.11), we finally obtain the relation

$$[(2\nu-1)\mu - P] \left[\frac{2}{\mu(\mu+P)} - \frac{1}{\mu_P}[2/\mu_P - \cot(\mu_P/2)] \right] = 0 , \quad \text{(B5)}$$

whose first solution is $\mu = P/(2\nu-1)$. Note that this result is not modified by surface tension.

In the viscous fingering case, one can first check (by considering P times the integral over the liquid domain Σ of the Green's function G) that

$$\mathrm{Re}(Z_+ + Z_-) = \mathrm{Re}(Y_+ - Y_-) .$$

The asymptotic expressions of $\mathrm{Re}Z_\pm$ are still given by (B2) and (B3), but $\mathrm{Re}Y_+^*$ is no longer subdominant and we find

$$\mathrm{Re}Y_+^*(x_0) \sim \pi\sigma\mu^2 A \left[(2\lambda-1) + \frac{\sin[(2\lambda-1)\mu/2]}{\sin(\mu/2)} \right] e^{-\mu x_0} . \quad \text{(B6)}$$

Using these asymptotic behaviors in the integral equation, one gets for the Saffman-Taylor problem [if we discard the spurious solutions $\mu = (2n+1)\pi/\lambda$]

$$\sigma\mu^2 = \cot[(1-\lambda)\mu/2] ,$$

which is identical to the relation $\cot\pi\tau = \kappa\tau^2$ obtained by McLean and Saffman,[13] where the correspondence between the notations is

$$\kappa = \frac{4\pi^2\sigma}{(1-\lambda)^2}, \quad \tau = \frac{(1-\lambda)\mu}{2\pi} .$$

2. $K<1$

This case is much easier; here we look for an asymptotic behavior of the form

$$y(x) \sim \tfrac{1}{2} - Ax^{-\beta} \quad \text{(B7)}$$

for x large. The dominant terms are then only $I_1(x_0)$ and $I_3(x_0)$:

$$I_1(x_0) \sim -\frac{A}{\beta-1} x_0^{1-\beta}, \quad I_3(x_0) \sim -\frac{A}{P} x_0^{1-\beta} ,$$

so we obtain, by substituting in (3.11), $\beta = 1/(1-K)$.

[1] S. de Cheveigné, C. Guttmann, and M. M. Lebrun, J. Phys. (Paris) **47**, 2095 (1986); H. Jamgotchian, B. Billia, and L. Capella, J. Cryst. Growth **82**, 342 (1987); **85**, 318 (1987); M. A. Eshelman, V. Seetharaman, and R. Trivedi, Acta Metall. **36**, 1165 (1988); V. Seetharaman, M. A. Eshelman, and R. Trivedi, *ibid.* **36**, 1175 (1988); A. Simon, J. Bechhoefer, and A. Libchaber, Phys. Rev. Lett. **61**, 2574 (1988).

[2] W. W. Mullins and R. F. Sekerka, J. Appl. Phys. **35**, 444 (1964).

[3] J. S. Langer, Rev. Mod. Phys. **52**, 1 (1980); in *Lectures in the Theory of Pattern Formation in Chance and Matter,* Les Houches XLVI, 1986, edited by J. Souletie, R. Stora, and J. Vannimenus (Elsevier, New York, 1987); D. A. Kessler, J. Koplik, and H. Levine, Adv. Phys. **37**, 255 (1988); P. Pelcé, *Dynamics of Curved Fronts* (Academic, London, 1988).

[4] J. S. Langer and L. A. Turski, Acta Metall. **25**, 1113 (1977); G. Dee and R. Mathur, Phys. Rev. B **27**, 7073 (1983); L .H. Ungar and R. A. Brown, *ibid.* **29**, 1367 (1984); **30**, 3993 (1984); **31**, 5923 (1985); **31**, 5931 (1985).

[5] D. A. Kessler and H. Levine, Phys. Rev. A **39**, 3041 (1989); **39**, 3208 (1989).

[6] M. Ben Amar and B. Moussallam, Phys. Rev. Lett. **60**, 317 (1988).

[7] T. Dombre and V. Hakim, Phys. Rev. A **36**, 2811 (1987); M. Ben Amar, T. Dombre, and V. Hakim, in *Propagation in Systems Far From Equilibrium,* Proceedings of the Les Houches Summer School of Theoretical Physics, 1987, edited by J. E. Wesfried, H. R. Brand, P. Manneville, G. Albinet, and N. Bocara (Springer-Verlag, Berlin, 1988).

[8] P. G. Saffman and G. I. Taylor, Proc. R. Soc. London, Ser. A **254**, 312 (1958).

[9] P. Pelcé and A. Pumir, J. Cryst. Growth **73**, 357 (1985).

[10] B. Billia, H. Jamgotchian and L. Capella, J. Cryst. Growth (to be published).

[11] J. D. Hunt, in *Solidification and Casting of Metals* (The Metals Society, London, 1979).

[12]B. I. Shraiman, Phys. Rev. Lett. **56**, 2028 (1986); D. C. Hong and J. S. Langer, *ibid.* **56**, 2032 (1986); R. Combescot, T. Dombre, V. Hakim, Y. Pomeau, and A. Pumir, *ibid.* **56**, 2036 (1986); R. Combescot, V. Hakim, T. Dombre, Y. Pomeau, and A. Pumir, Phys. Rev. A **37**, 1270 (1988).

[13]J. W. McLean and P. G. Saffman, J. Fluid Mech. **102**, 455 (1981); J. M. Van den Broeck, Phys. Fluids **26**, 2033 (1983).

[14]D. A. Kessler, J. Koplik, and H. Levine, Phys. Rev. A **34**, 4980 (1986); A. Dorsey and O. Martin, *ibid.* **35**, 3989 (1987).

[15]Y. Pomeau, Stud. Appl. Math. **73**, 75 (1985).

[16]P. Pelcé has pointed out to us that he had also obtained this relation in a collaborative work with A. Karma, Phys. Rev. A **39**, 4162 (1989).

[17]B. Billia, H. Jamgotchian, and L. Capella, J. Cryst. Growth **82**, 747 (1987); **94**, 987 (1989).

[18]H. Esaka and W. Kurz, J. Cryst. Growth **72**, 578 (1985); H. Esaka, Ph.D. thesis, Ecole Polytechnique Féderate de Laussan, 1986; H. Jamgotchian, B. Billia, and L. Capella, J. Cryst. Growth **64**, 338 (1983).

[19]C. Guthman (unpublished).

[20]J. D. Weeks and W. van Saarlos, Phys. Rev. A **39**, 2772 (1989).

[21]D. Meiron, Phys. Rev. A **33**, 2704 (1986); D. Kessler, J. Koplic, and H. Levine, Phys. Rev. A **33**, 3352 (1986); M. Ben Amar and B. Moussallam, Physica D **25**, 155 (1987).

[22]A. Karma, Phys. Rev. Lett. **57**, 858 (1986).

[23]*Table of Integrals, Series and Products,* edited by I. S. Gradshteyn and I. M. Ryzhik (Academic, London, 1980).

[24]L. Landau and B. Levich, Acta Physicochim. **17**, 42 (1942).

[25]*Handbook of Mathematical Functions,* edited by M. Abramovitz and I. A. Stegun (Dover, New York, 1970).